Recombinative desorption dynamics: Molecular hydrogen from Cu(110) and Cu(111)

G. D. Kubiak,[a] G. O. Sitz, and R. N. Zare[b]
Department of Chemistry, Stanford University, Stanford, California 94305

(Received 27 February 1985; accepted 14 May 1985)

The rotational and vibrational distributions of H_2 and D_2 recombinatively desorbing from clean Cu(110) and Cu(111) surfaces following atomic permeation are studied using multiphoton ionization combined with time-of-flight mass spectrometry. Rotational distributions are found to be non-Boltzmann and to possess mean rotational energies which are 80%–90% of the surface temperature, T_s. These distributions are identical to within the experimental accuracy for H_2 and D_2 and also for desorption from the (110) and (111) faces. Moreover, the ortho and para nuclear spin modifications of both isotopes are statistically populated. In contrast, the vibrational population ratio, $P_{v''=1}/P_{v''=0}$, is found to be as much as 100 times greater than the ratio corresponding to a Boltzmann vibrational population at T_s. Specifically, the $P_{v''=1}/P_{v''=0}$ ratio for H_2 (D_2) is 0.052 ± 0.014 (0.24 ± 0.20) desorbing from Cu(110), and 0.084 ± 0.030 (0.35 ± 0.20) desorbing from Cu(111). For comparison the Boltzmann-at-T_s ratios would be 0.0009 for H_2 and 0.0063 for D_2 at $T = 850$ K. Simple models are discussed which attempt to account for the qualitative trends of these results. Detailed balance arguments applied to the vibrational distributions measured in recombinative desorption are unable to predict correctly the dissociative adsorption probability as a function of vibration, indicating that these two processes are dynamically different for this system.

I. INTRODUCTION

In the desorption of gases from surfaces, the escaping species are commonly described by a Boltzmann distribution at the surface temperature, T_s. However, there are some outstanding exceptions.[1] One such case is the activated recombinative desorption of hydrogen from copper.[2–7] The reverse process, dissociative adsorption, also shows strong variations of the sticking probability as a function of incident velocity and angle[8] for this system. When desorption or adsorption processes show such nonequilibrium behavior, then a detailed study of the quantum state distributions may yield information regarding the dynamics of these simple heterogeneous reactions.

The adsorption of molecular hydrogen on copper was first demonstrated to be activated and dissociative by Pritchard and co-workers,[9–12] who studied adsorption on evaporated copper films. They found isosteric heats of adsorption for H_2 in the range of 10–12 kcal/mol on these polycrystalline samples and an activation energy for dissociative chemisorption of approximately 9 kcal/mol. More recently, results of Wachs and Madix[13] have shown that the second order preexponential factor for D atoms recombinatively desorbing from Cu(110) is approximately 10^4 times smaller than typical values on other metals. This suggests that unusual dynamics control the escape of D_2 from the surface. The important role of the dynamics was demonstrated by Balooch and Stickney[3] who found that the recombinative desorption flux of H_2 from the three low index faces of Cu exhibited angular distributions which were strongly peaked along the surface normal. The distributions could empirically be fit to the form $\cos^n \theta$ where n values were 2.5, 5, and 6 for the (110), (100), and (111) faces, respectively. These workers tentatively ascribed their observations to a model originally suggested by Lennard-Jones[14] in which a potential curve-crossing between atomic and molecular potentials is thought to occur above the surface.

Supporting evidence was presented in a beautiful experiment by Balooch, Cardillo, Miller, and Stickney[8] who determined dissociative adsorption probabilities of H_2 and D_2 on the (100), (110), and (310) faces of Cu as a function of incident molecular velocity and angle. They found that the activation barriers to dissociative adsorption could be surmounted by the incident kinetic energy projected along the surface normal, suggesting that the barriers associated with the translational degree of freedom were approximately one dimensional. This had originally been proposed by van Willigen.[15] Values of 3, 5, and 5 kcal/mol for these barrier heights were assigned to the (110), (100), and (310) faces, respectively.

Cardillo, Balooch, and Stickney[5] later analyzed these results using detailed balance. This approach assumes that the microscopic rate of desorption into a given state is equal to the reverse rate of adsorption from that state. They used the angle and velocity dependence of the sticking probability[8] to predict successfully the velocity-integrated post-permeation desorption angular distributions.[3] Indeed, calculations employing detailed balance have proven useful in a number of gas–surface reactions.[16]

More recently, Comsa and David[4] have measured the velocity distributions of D_2 recombinatively desorbing from the (111) and (100) faces of Cu following atomic permeation. They found that the correlation expected between velocity and desorption angle for the simplest one-dimensional barrier model did not exist, i.e., the velocity did not increase with increasing angle from the surface normal. Their results seem to contradict the detailed balance arguments of Cardillo *et al.*,[5] suggesting that post-permeation recombinative

[a] Present address: Surface Science and Chemical Physics Division, Sandia National Laboratories, Livermore, CA 94550.
[b] Holder of a Shell Distinguished Chair.

 0021-9606/85/172538-14$02.10

desorption is governed by different potentials than is dissociative adsorption.

In the present study we measure the rovibrational distribution of H_2 and D_2 recombinatively desorbing after atomic permeation through Cu(111) and Cu(110). We find that the rotational distributions are non-Boltzmann. They have a mean energy slightly less than the surface, and this quantity is independent of crystal face and isotopic variation. On the other hand, the $P_{v''=1}/P_{v''=0}$ population ratio is dramatically increased over that expected for equilibrium at T_s. Various simple models are considered for interpreting these findings. The validity of detailed balance is critically examined by calculating the dynamics in the adsorption direction from our desorption results, and comparing these predictions to existing results. We present further evidence that detailed balance is unable to relate correctly dissociative adsorption and post-permeation recombinative desorption for the $H_2(D_2)$/Cu system.

II. EXPERIMENTAL

A schematic diagram of the apparatus is depicted in Fig. 1. The basic experimental procedure will only be summarized, as detailed descriptions of each important apparatus element may be found elsewhere.[7,17] Recombinative desorption fluxes of H_2 and D_2 are provided by atomic permeation from a pressurized gas line (1–3 atm) through heated single-crystal copper sample membranes having nominal thicknesses of 0.5 mm. Sample cleanliness and geometric order are accomplished by Ar^+ bombardment and annealing cycles and are verified by Auger electron spectroscopy (AES) and low energy electron diffraction (LEED), respectively. The desorption flux is crossed by a 3 ns pulsed laser beam

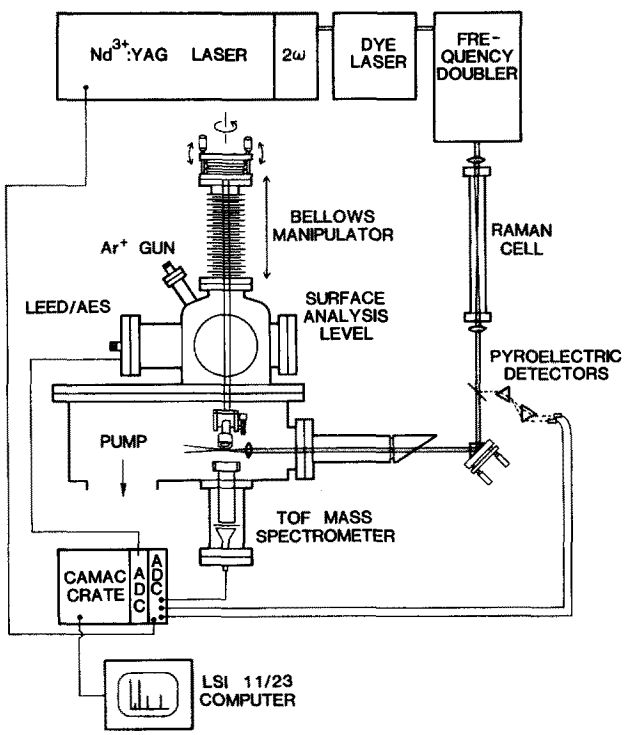

FIG. 1. Diagram of the overall experimental apparatus used to determine rovibrational state distributions of molecular hydrogen desorbing from clean copper surfaces.

focused approximately 1.25 cm from the sample surface and is ionized via resonance enhanced 2 + 1 multiphoton ionization.[18] Ions are extracted into a time-of-flight mass spectrometer. Mass segregation occurs due to differences between ion mass flight times which are proportional to the square root of a given ion's mass. Ions are detected with a high-gain multiplier array as a function of laser wavelength to obtain an ionization spectrum. Comparison of the vibrationally and rotationally resolved line intensities of the desorbing species with those from an oven source allows the rovibrational state populations to be determined.

A. Single-crystal permeation source

The (110) sample permeation source consists of a single-crystal Cu cylinder, 99.999% pure 1.25 cm long, and 1.25 cm in diameter. An interior 3 mm channel is electro-discharge milled to within 0.8 mm of the oriented cylinder front face. This face is oriented to within 1° of the (110) plane as quoted by the crystal manufacturer (Monocrystals Co., Cleveland, OH). Electro-discharge milling was chosen for channel construction to avoid creating defects in the sample substrate, a problem to which copper is extremely susceptible due to its softness.[19] The (111) sample source was constructed using a slightly different procedure in which an oriented (1°) 99.999% pure, 1 cm diameter, 1 mm thick disk was electron beam welded to a channeled, 99.999% purity cylinder. After welding, the disk was sanded carefully and chemically etched to a final 0.3 mm thickness.

The Cu sample surfaces were both chemically polished to mirror finishes using the method of Mitchell and Ahearn,[20] although the (111) face had to be repolished at a later time with 0.25 μ diamond paste due to a scratch. Both faces yielded high contrast LEED patterns after sputtering and annealing, although the (111) face required a much longer annealing period, presumably due to the use of a mechanical rather than chemical final polish.

At a surface temperature of 900 K, a sample thickness of 1 mm, and an H_2 backing pressure of 1 atm, the calculated desorption flux is 9×10^{13} molecules/cm^2 s. This corresponds roughly to a density of 1×10^{-8} molecules/cm^3 assuming that the mean H_2 velocity is 8×10^5 cm/s. Under these conditions the hydrogen coverage is calculated to be less than 10^{-4} of a monolayer. Hence, the post-permeation desorption measurements are performed in the zero-coverage limit.

B. Laser excitation and ion detection

For two-photon excitation of the H_2 $E, F\,^1\Sigma_g^+$ state the wavelength combinations employed are 193 and 211 nm for the (0,0) band and 2×211 nm for the (0,1) band, enabling spectra of both vibrational bands to be acquired simultaneously. The laser source is comprised of a pulsed dye laser (Quanta-Ray, PDL) with single stage amplifier, pumped by the frequency-doubled output of a pulsed Nd^{3+}:YAG laser (Quanta-Ray, DCR-1A). The doubled dye output, tunable in the region near 285.63 nm, is focused with an $f = 600$ mm quartz lens into a cell containing 5.5 atm of H_2 gas. Stimulated Raman scattering occurs within the focal volume to produce wavelengths of light which are shifted by integral mul-

tiples of the H_2 Q_1 vibrational quantum of 4155.0 cm^{-1}. The third and fourth anti-Stokes lines, denoted by AS_3 and AS_4, are generated at 211 and 193 nm, respectively. Table I lists the relevant operating conditions.

The input lens is an uncoated $f = 600$ mm quartz lens which focuses both the dye (vertically polarized) and doubled dye (horizontally polarized) laser wavelengths within the 72 cm Raman cell.[21] A 500 mm Suprasil lens recollimates the output which is sent without dispersion to a beam splitter and then to a beam-steering prism. The prism is mounted on a precision mount so that accurate beam steering into the chamber is possible. The beam splitter picks off ~8% of the undispersed Raman cell output and sends it to two matched 60° dispersing prisms placed so that the second prism is in the mirror image configuration to the first. In this way, the AS_3 and AS_4 orders can be spatially separated without beam walking during a dye laser wavelength scan. The beams at ~193 and ~211 nm are then mildly focused on separate pyroelectric detectors (Molectron P1-12) which produce currents that are linearly proportional to pulse energy. The pyroelectric outputs are amplified with fast 10× pre-amps (LeCroy VV100BTB) and sent to a gated integrator/computer system for power normalization. Inside the chamber the two laser wavelengths at ~193 and ~211 nm are focused with a 75 mm focal length Suprasil lens. These wavelengths have slightly displaced foci, but the degree to which the two colors do not overlap is fairly small.

As shown in Fig. 2, ions formed at the laser foci are accelerated into a 16 cm long time-of-flight mass spectrometer tube by an extraction field of ~400 V/cm. A channel electron multiplier array (CEMA, Galileo FTD 2002) lies 1 cm below the exit grid of the flight tube and is used to detect the temporally resolved ions which strike it. Temporal discrimination of the ion masses is critical in this experiment, even at pressures of 10^{-10} Torr, because of the abundant nonresonant production of background hydrocarbon masses in the tightly focused ionization region. Typical mass resolution, $t/\Delta t$, is about 30 in a time-of-flight spectrum. H_2^+ flight times are ~1.5 μs.

The output of the CEMA is processed by gated integration (LeCroy models 2249SG and 2323) in a CAMAC crate and is stored in a computer (DEC LSI 11/23). A resonance-enhanced multiphoton ionization (REMPI) spectrum is obtained by tuning the wavelength of the laser while integrating the CEMA output at the fixed delay from the laser pulse appropriate to the desired mass. Because the spectrum is so sparse, the data acquisition program scans the dye laser quickly through empty regions of the spectrum and slowly through regions where transitions occur. Spectra are acquired in 45 min scans following hour-long Ar^+ bombardment at an ion energy of 1000 eV and a current density of ~3 $\mu A/cm^2$. Three sequential scans are performed after which point an AES spectrum is taken. The Auger spectra show that small amounts of carbon accumulate on the sample surface during data acquisition [I_C(272 eV)/I_{Cu}(920 eV)≅1] but this seems to have no effect on the rovibrational state distributions.

TABLE I. Implementation of stimulated Raman scattering for H_2, D_2 detection.

Scattering gas:	H_2
Gas pressure:	65 psig
Focal length of input focusing lens:	600 mm
Dye wavelength:	571.23 nm
Dye energy:	70 mJ/pulse
Doubled dye energy:	18 mJ/pulse
AS_4 wavelength:	193.68 nm
AS_4 energy:	118 μJ/pulse
AS_3 wavelength:	210.63 nm
AS_3 energy:	311 μJ/pulse

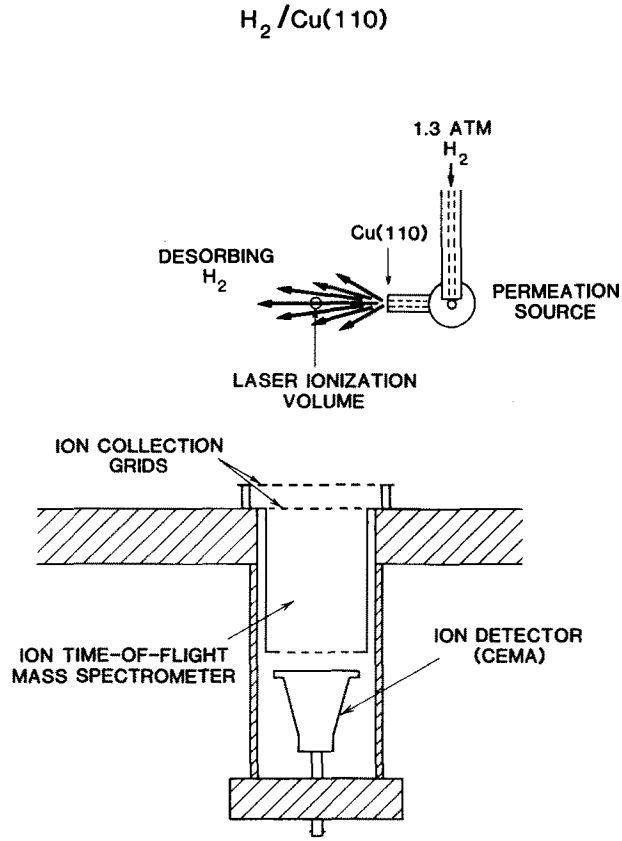

FIG. 2. Time-of-flight mass spectrometer used to collect laser-ionized molecular hydrogen.

III. RESULTS

A. H_2 and D_2 rovibrational population standards

The general use of REMPI to determine quantum state populations requires that both the excitation and ionization steps be fully characterized. Toward that end REMPI spectra of both H_2 and D_2 supplied by a 25 μ heated tungsten free jet have been recorded as a function of the stagnation temperature. These measurements are compared with the results of Gallagher and Fenn[22] who studied rotational relaxation of molecular hydrogen in heated free jets. In this way, the accuracy of the methods adopted for rotational population analysis may be verified. Moreover, the nozzle can be used as a source of well-defined vibrational distributions to calibrate the REMPI technique for use in vibrational population analysis.

The nozzle is resistively heated along approximately 5 cm of its length and the resulting temperature, T_0, is mea-

sured with a W–5% Re/W–26% Re thermocouple spot-welded 2 cm behind the nozzle orifice. Hydrogen flows are sufficiently slow that molecular dwell times within the heated region of approximately 0.5 s are expected. The 10^{11} collisions which each molecule is calculated to experience during this time ensures that full rotational and vibrational equilibration to the source temperature is achieved. The source is mounted so as to provide three translational degrees of freedom, allowing molecular beam alignment to be dynamically maintained during experiments. The nozzle and its associated manipulation hardware are mounted in a triply differentially pumped source chamber assembly previously described.[23]

Rotational relaxation of molecular hydrogen in a jet has been studied using time-of-flight methods by Gallagher and Fenn.[22] We have employed stagnation conditions which, according to their measurements, yield terminal rotational temperatures, T_r, equal to 0.9 T_0. Vibrational temperatures, T_v, are expected to be at least this high,[22] but are probably even greater. Ordinarily it can be safely assumed that $T_v = T_0$ for light diatomics. The possibility of near-resonant vibration to rotation energy transfer has been suggested for H_2,[24] however, and so we adopt the position of Gallagher and Fenn on this point and tentatively assume that $T_v \sim T_r$.

Examples of both H_2 and D_2 REMPI spectra are shown in Fig. 3 for the stagnation conditions as listed. Such data were collected only for stagnation pressures of 1 atm for H_2 and 2 atm for D_2. Notice the prominent $v'' = 1$ signal. Because the pulse energy of AS_3 is generally three times greater than that of AS_4 and since their foci do not exactly overlap, the relative detection sensitivity for $v'' = 1$ is far greater than that for $v'' = 0$. These spectra are analyzed in the following manner: (1) each Q-branch J member which is not overlapped with another line is integrated and any underlying background is subtracted, and (2) the integrated intensity, denoted as IQ_J, is divided by the product of the simultaneously measured laser pulse energies (e.g., $AS_3 \cdot AS_4$ for $v'' = 0$ detection), and by the combined nuclear and rotational degeneracies appropriate to the state J. In general, these ratios must also be divided by the corresponding two-photon transition line strengths (see for example Bray and Hochstrasser[25]). Previous measurements[18(b)] have demonstrated that the second rank contribution to the $^1\Sigma_g^+ \leftarrow {}^1\Sigma_g^+$ two-photon line strength is small and therefore the J dependence of the overall line strength is weak. To a good approximation ($\sim 1\%$) therefore, these quantities need not be included. The power and degeneracy normalized intensities are plotted logarithmically vs the rotational energy E_J of the state J. The resulting Boltzmann plots are presented in Fig. 4 for H_2 $v'' = 0$ and in Fig. 5 for D_2 $v'' = 1$.

These two figures show that:

(i) the data for all T_0 are well described by straight lines, implying that the distributions are Boltzmann and can be accurately fit by rotational temperatures, T_r;

(ii) the values of T_r, summarized in Table II, are typically within 10% of and are systematically lower than T_0;

(iii) the ratio of T_r/T_0, averaged over all values of T_0, is 0.94 ± 0.15 for H_2 and 0.89 ± 0.08 for D_2, very close to the value of 0.9 expected from the results of Gallagher and Fenn.[22]

As a final test, we analyze a room temperature static gas sample of H_2 and obtain $T_r = 298 \pm 3$ K when the chamber temperature is 295 K. These results demonstrate that rota-

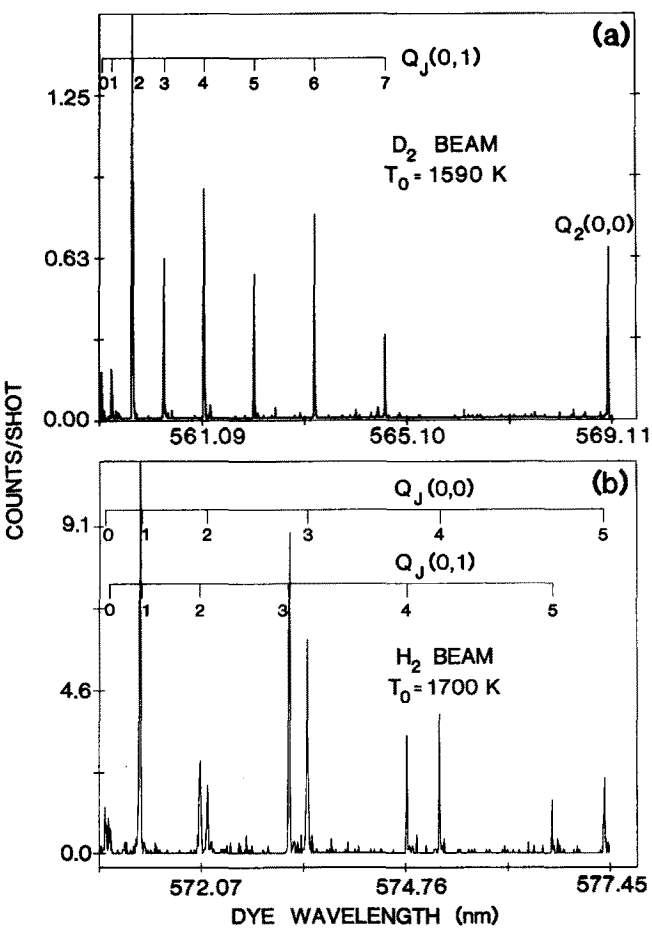

FIG. 3. Resonance-enhanced multiphoton ionization spectra of (a) H_2 and (b) D_2 expanded from the nozzle. The stagnation temperature, T_0, is as listed. The stagnation pressure, P_0, is 1 atm for H_2 and 2 atm for D_2.

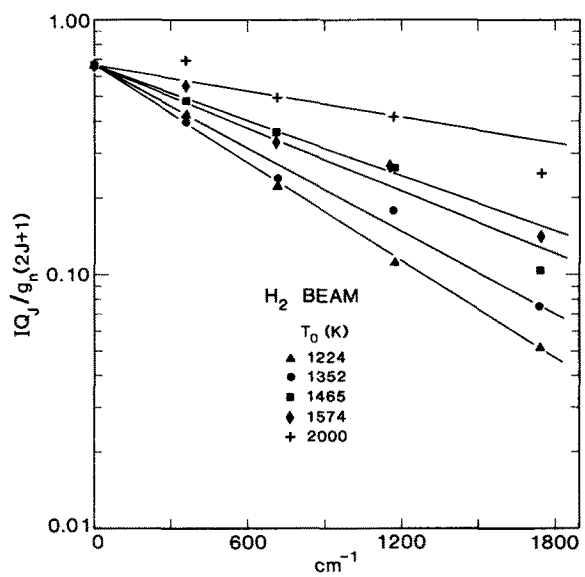

FIG. 4. Boltzmann plot of jet-expanded H_2, $v'' = 0$. The ordinate is the logarithm of the laser power- and degeneracy-normalized rotational line intensities and the abscissa is E_J, the rotational energy. Values of T_0 and T_r are listed in Table II.

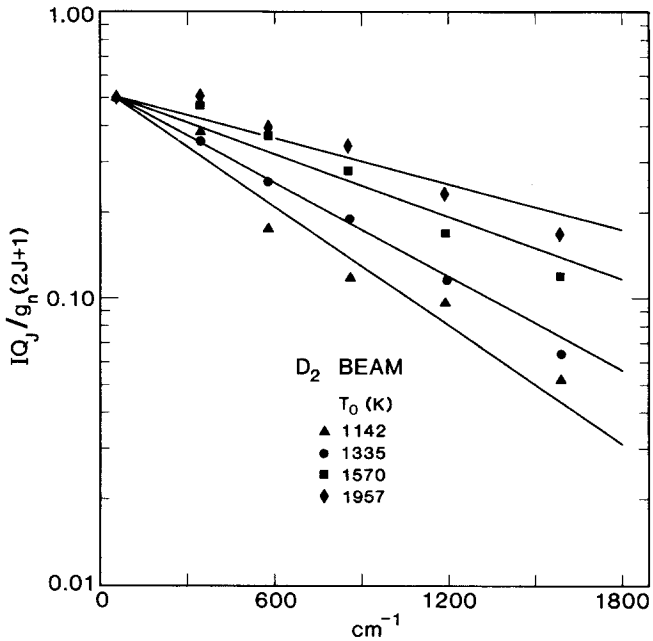

FIG. 5. Boltzmann plot of jet-expanded D_2, $v''=1$. Values of T_0 and T_r are listed in Table II.

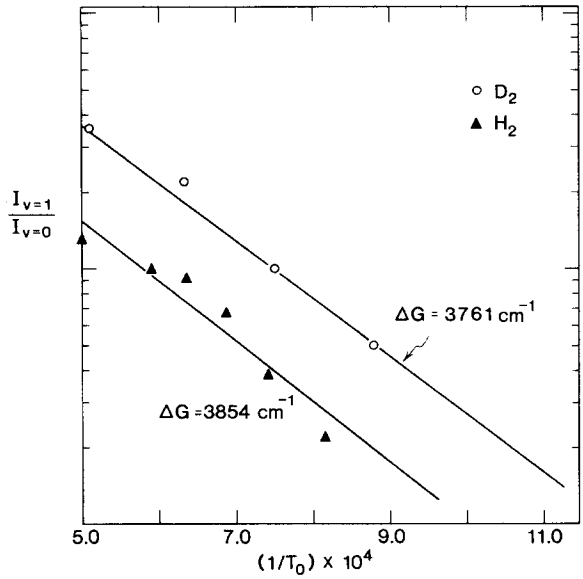

FIG. 6. Logarithmic plot of the $(v''=1)/(v''=0)$ intensity ratio vs $(T_0)^{-1}$ for jet-expanded H_2 and D_2. The lines drawn correspond to the least squares fits to the data.

tional population determinations can be accurately accomplished using REMPI of molecular hydrogen. However, since we have not verified our procedures for transitions involving $J>5$ for H_2 and $J>7$ for D_2, in all results which follow we use only those rotational transitions which have been shown to be free from any possible J-dependent detection bias.

To calibrate REMPI detection of molecular hydrogen vibrational populations we have used the nozzle source as a vibrational population standard. Recall that T_v is expected to be at least 0.9 T_0. A calibration curve is developed vs T_0 by measuring the signal intensity in selected $Q(0,1)$ and $Q(0,0)$ members and determining the population ratio

$$\frac{P_{v''=1}}{P_{v''=0}} = \frac{\sum_J IQ_J(0,1)}{\sum_J IQ_J(0,0)}, \tag{1}$$

where the range of J is $2 \leqslant J \leqslant 5$ for H_2 in both v'' levels and is $J=2$ for $v''=0$ of D_2, and $0 \leqslant J \leqslant 7$, $J \neq 2$ (because of line blending), for $v''=1$ of D_2. The ratio formed for D_2 is multiplied by the quantity

$$\frac{P_{v''=0,J=2}(T_0)}{\sum_J P_{v''=0,J}(T_0)}$$

TABLE II. Values of T_r as a function of T_0 for H_2 and D_2.

H_2 ($v''=0$)		D_2 ($v''=1$)	
T_0(K)	T_r(K)	T_0(K)	T_r(K)
1224	961	1142	964
1352	1209	1335	1062
1465	1326	1578	1502
1575	1445	1957	1876
1693	1621		
2015	2430		
$\langle T_r/T_0 \rangle$	0.94 ± 0.15	$\langle T_r/T_0 \rangle$	0.89 ± 0.08

to correct for the decrease in partition function-normalized population in $J=2$, $v''=0$, denoted by $P_{v''=0,J=2}$, as temperature increases. The logarithms of the ratios expressed in Eq. (1) vs $(T_0)^{-1}$ are plotted for H_2 and D_2 in Fig. 6. To a good approximation these plots yield straight lines and their resulting slopes are equal to within 10%–20% of the energy difference, $E_{v''=1} - E_{v''=0}$. This is the expected result when full molecular vibrational equilibration to T_0 occurs and vibrational relaxation in the jet is either insignificant or independent of T_0. Combined with the assumption that $T_v \sim T_r$ (in our view, a lower limit), we conclude that the true vibrational population ratio can be predicted to within 10% from knowledge of T_0.

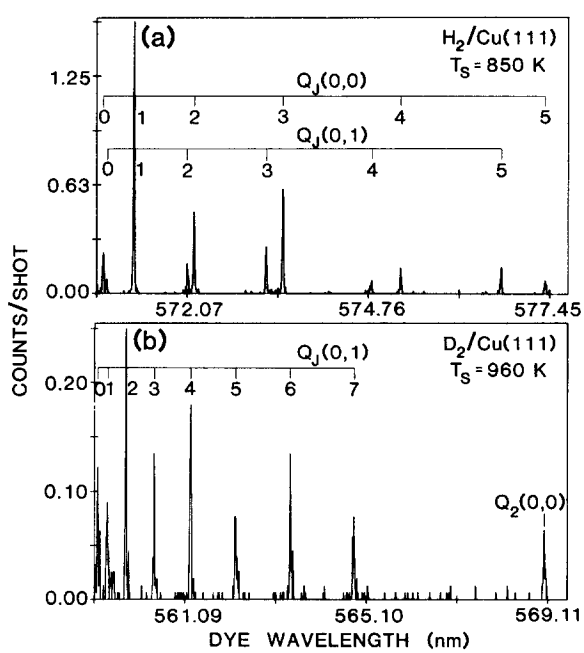

FIG. 7. Resonance-enhanced multiphoton ionization spectra of (a) H_2 desorbing from Cu(111) at $T_s = 850$ K and (b) D_2 desorbing from Cu(111) at $T_s = 960$ K.

B. Rotational distributions in post-permeation desorption

Representative spectra of H_2 and D_2 desorbing from Cu(111) are shown in Fig. 7 at the specified values of T_s. All spectra of recombinatively desorbing molecular hydrogen are collected such that they represent an average over desorption angles ranging from 0°–20° from the surface normal. No attempts have been made to search for correlations between desorption angle and internal state. Similarly, possible effects of anisotropy of molecular rotational angular momentum have been ignored. For future reference, we have chosen a detection geometry in which the angle between the surface normal and laser polarization direction is fixed at approximately 40°.

To prove unambiguously that spectra such as those in Fig. 7 correspond to the direct flux of recombinative desorption from the clean sample surface we have performed two tests. The first test is to determine the spatial profile of the signal at $Q_3(0,1)$. We find this peaks near the surface normal, as expected. As a second test the copper surface is contaminated with sulfur through exposure to H_2S. We find that the recorded spectra change drastically.[7]

The background $H_2(D_2)$ pressure in the vacuum chamber increases to approximately 5×10^{-9} Torr during a permeation run and this diffuse background component contributes significantly to the signal measured along the permeation flux spatial maximum. We subtract this contribution after each set of three scans in a manner which assumes that the background molecules have an equilibrium rovibrational distribution at the chamber temperature of 295 K (i.e., there is no background contribution to the $v''=1$ signal). This assumption is based on the fact that desorbed molecules on average undergo many wall collisions before returning it to the ionization region.

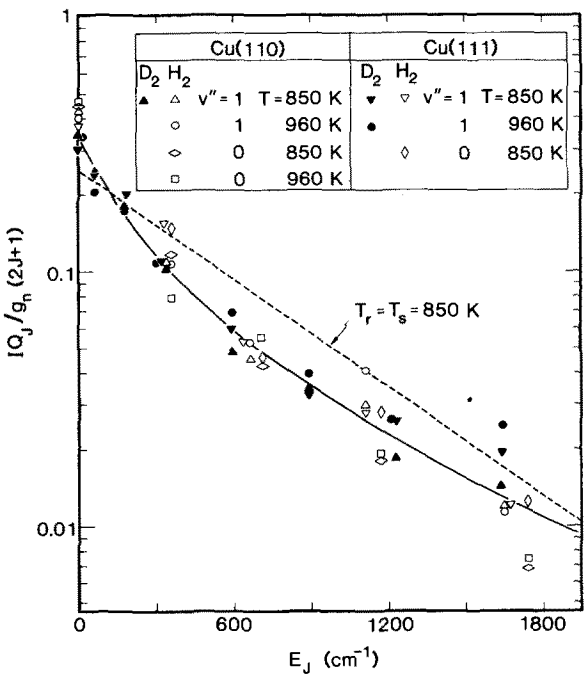

FIG. 8. Boltzmann plot of H_2 and D_2 recombinatively desorbing from Cu(110) and Cu(111). The dashed line $T_r = T_s = 850$ K is drawn for reference. The curve through the data is simply to aid the eye.

Following background subtraction, rotational analyses for both $v''=0$ and $v''=1$ are performed as described above for the heated nozzle data. The results are plotted for both H_2 and D_2 desorbing from Cu(110) and Cu(111) in Fig. 8. Data were collected at two values of T_s for each surface and these results are plotted as well. Figure 8 is a plot of the logarithm of the quantity $IQ_J/[g_n(2J+1)]$ vs E_J, where IQ_J is the power-normalized intensity of the Q branch member, g_n is the nuclear spin degeneracy, $(2J+1)$ is the corresponding rotational degeneracy, and E_J is the rotational energy, all of the state J. The line corresponding to $T_r = T_s = 850$ K is included in this figure for reference. The following conclusions may be immediately drawn from Fig. 8:

(i) the H_2 and D_2 rotational distributions are not accurately represented by a temperature although the deviation from Boltzmann behavior is not dramatic;

(ii) the mean rotational energy is less than T_s;

(iii) the H_2 and D_2 distributions are identical to within the accuracy of the data;

(iv) the Cu(110) data are identical to the Cu(111) data to within the experimental accuracy;

(v) the H_2 data for $v''=0$ and $v''=1$ show no systematic differences (this comparison cannot be made for D_2 because the signal in $v''=0$ is too weak to allow its characterization);

(vi) ortho and para modifications of both H_2 and D_2 lie along common curves, implying they are populated statistically;

(vii) no systematic differences are noted for the two surface temperatures studied.

Tables III and IV list the normalized rotational populations for all of the data appearing in Fig. 8. Also tabulated is the quantity $\langle E_r\rangle/\langle E_r(T_s)\rangle$. This ratio corresponds to the mean rotational energy in recombinative desorption, $\langle E_r\rangle$, divided by the mean rotational energy predicted for equilibrium at T_s, $\langle E_r(T_s)\rangle$. Error estimates are included parenthetically after each data entry.

C. Vibrational distributions in post-permeation desorption

Examination of Fig. 7 demonstrates that the vibrational excitation of the desorbing hydrogen is substantially greater than the amount that would be expected for equilibrium at T_s. A coarse estimate of the $v''=1$ population may be gained simply by comparing the H_2 spectra in Figs. 3 and 7. We note that the temperature of the beam source is almost twice that of the surface and yet the relative fraction of $v''=1$ is only slightly less in the desorption spectrum than in the beam spectrum.

The quantitative determination of the vibrational population ratio, $P_{v''=1}/P_{v''=0}$, is established by first subtracting off the background contribution to the $v''=0$ signal as described above. The remainder of the procedure differs slightly for H_2 compared to D_2. In the case of H_2, the sum over power-normalized Q_2 to Q_5 lines is determined for both members of the v'' progression (0 and 1) and the ratio calculated. This empirical ratio is then entered as the variable in the equation of the best-fit line to the free jet data appearing

TABLE III. Normalized rotational populations for H_2 desorption. Also tabulated are the resulting mean rotational energies divided by the equilibrium-at-T_s prediction.

	$T_s = 850$ K		$T_s = 960$ K	
H_2/Cu(110)	$v'' = 0$	$v'' = 1$	$v'' = 0$	$v'' = 1$
J	P_J			
0	0.19(0.11)	0.15(0.06)	0.19(0.11)	0.14(0.03)
1	...	...	...	...
2	0.25(0.06)	0.21(0.03)	0.16(0.05)	0.21(0.03)
3	0.39(0.07)	0.38(0.04)	0.50(0.07)	0.39(0.03)
4	0.07(0.02)	0.09(0.02)	0.07(0.04)	0.13(0.04)
5	0.10(0.01)	0.16(0.06)	0.10(0.06)	0.13(0.01)
$\frac{\langle E_r \rangle}{\sum_{J(J\neq 1)} P_J(T_s)\cdot E_J}$	0.81	0.91	0.77	0.81

	$T_s = 850$	
H_2/Cu(111)	$v'' = 0$	$v'' = 1$
J	P_J	
0	0.29(0.17)	0.12(0.05)
1	...	...
2	0.23(0.11)	0.27(0.07)
3	0.29(0.11)	0.39(0.06)
4	0.07(0.05)	0.09(0.03)
5	0.12(0.05)	0.14(0.06)
$\frac{\langle E_r \rangle}{\sum_{J(J\neq 1)} P_J(T_s)\cdot E_J}$	0.76	0.90

in Fig. 6 and the true population ratio calculated. The D_2 ratio is determined in a similar manner which accounts for the change in the fractional population in $J = 2$ as a function of temperature.[17] We find that the vibrational population ratios in desorption are 0.052 ± 0.014 and 0.24 ± 0.20 for H_2 and D_2, respectively, from Cu(110). On the Cu(111) surface these ratios are 0.084 ± 0.030 for H_2 and 0.35 ± 0.20 for D_2. In contrast, the vibrational population ratios in equilibrium at $T_s = 850$ K are 0.0009 and H_2 and 0.0063 for D_2. Note, therefore, that the activated recombinative desorption of molecular hydrogen results in vibrational excitation some 50 times the value predicted if the molecules were desorbing in equilibrium from Cu(110). On Cu(111) we see ~ 100 times the amount in $v'' = 1$ than the equilibrium prediction.

We have unsuccessfully attempted to measure the population in the $v'' = 2$ level following desorption for both H_2 and D_2. However, by measuring the $(v'' = 2)/(v'' = 0)$ signal ratio in the molecular beam at $T_0 = 2000$ K, upper limits of ~ 0.01 for H_2 and ~ 0.04 for D_2 can be established for the $v'' = 2$ desorption populations.

The normalized rotational populations presented in Tables III and IV may be combined with the vibrational population ratios presented above to yield relative rovibrational state populations. Such relative populations are graphed in Fig. 9 for H_2 and D_2 on Cu(111). To accentuate the differences between the measured quantum state populations and those predicted for an equilibrium ensemble at T_s, we also graph the ratio of the two populations. In this way, the dynamical aspects of desorption can be separated from the simple "thermal" predictions.

IV. DISCUSSION

As summarized in the Introduction, the activated recombinative desorption and dissociative adsorption of molecular hydrogen on copper surfaces exhibit clear nonequilibrium angular and velocity distributions. It is known that the activation barrier to dissociative adsorption is nominally one dimensional having a height that depends on the surface crystallographic orientation.[5] Moreover, velocity measurements suggest that there are dynamical differences between gas-phase adsorption and post-permeation desorption.[4]

The present study examines the role played by molecular internal degrees of freedom during recombinative desorption. Specifically we have determined the rovibrational state populations of molecular hydrogen desorbing after atomic permeation. We have made no attempt to determine the possible correlations between these internal degrees of freedom and desorption velocity or angle. Such experiments are possible in principle, but will require signal enhancements of approximately a factor of 10.

In desorption, molecules escaping the surface will exhibit state distributions which derive from at least two distinct paths. One path is the recombination of hydrogen atoms and the *direct* escape of molecules into the vacuum. The other involves recombination followed by collisions between the newly born molecule and one or more surface atoms. Presumably these collisions will tend to thermalize the direct path distributions. The detailed form of the potential energy as a function of v'', J, velocity, etc., determines which molecular quantum states contribute primarily to the direct desorption flux. In this sense, the copper surface acts

TABLE IV. Normalized rotational populations for D_2 desorption. Also tabulated are the resulting mean rotational energies divided by the equilibrium-at-T_s prediction.

D_2/Cu(110)	$T_s = 850$ K
	$v'' = 1$
J	P_J
0	0.12(0.04)
1	0.12(0.03)
2	0.28(0.06)
3	0.12(0.03)
4	0.15(0.04)
5	0.08(0.04)
6	0.09(0.03)
7	0.06(0.03)
$\frac{\langle E_r \rangle}{\sum_J P_J(T_s)\cdot E_J}$	0.93

D_2/Cu(111)	$T_s = 850$ K	$T_s = 960$ K
	$v'' = 1$	$v'' = 1$
J	P_J	P_J
0	0.09(0.03)	0.11(0.03)
1	0.11(0.03)	0.09(0.04)
2	0.31(0.04)	0.27(0.04)
3	0.12(0.02)	0.12(0.04)
4	0.16(0.05)	0.19(0.04)
5	0.05(0.02)	0.07(0.02)
6	0.10(0.03)	0.11(0.02)
7	0.04(0.02)	0.06(0.03)
$\frac{\langle E_r \rangle}{\sum_J P_J(T_s)\cdot E_J}$	0.86	0.88

as a quantum state "filter."

We assume in the following discussion that the "direct" desorption flux dominates the total desorption flux. Rotation is expected to be more sensitive to possible relaxation than is vibration, although both of these degrees of freedom should be more difficult to relax collisionally than velocity. We believe that the narrow, hot velocity distributions measured by Comsa and David[4] support the assumption that the direct flux is predominant. However, we cannot rule out a minor contribution to the desorption flux from a group of molecules with partially relaxed internal state distributions.

A. Features of the molecule–surface potential manifested in molecular rotation

The quantum state distributions of direct recombinatively desorbing hydrogen molecules will reflect the details of the potential energy surfaces governing the motions of the constituent H atoms and of the newly born H_2 molecules. These potential energy surfaces are expected to vary with the crystallographic orientation of the copper surface. Recall that such variations have already been observed in post-permeation desorption angular and velocity distributions, as well as in the apparent activation energy for dissociative adsorption. Specifically, H_2 angular distributions measured by Balooch and Stickney vary in the sequence $\cos^{2.5}\theta$, $\cos^5\theta$, and $\cos^6\theta$ for the (110), (100), and (111) surfaces, respectively.[3] More recent angular distributions, measured by Comsa and David,[4] yield $\cos^8\theta$ for Cu(100). D_2 velocity distributions in desorption from Cu(100) and Cu(111) yield mean kinetic energies of 3950 and 3600 K, respectively.[4] In adsorption, the apparent activation barrier varies from 3 kcal/mol on the (110) surface to 5 kcal/mol on the (100) plane.[8]

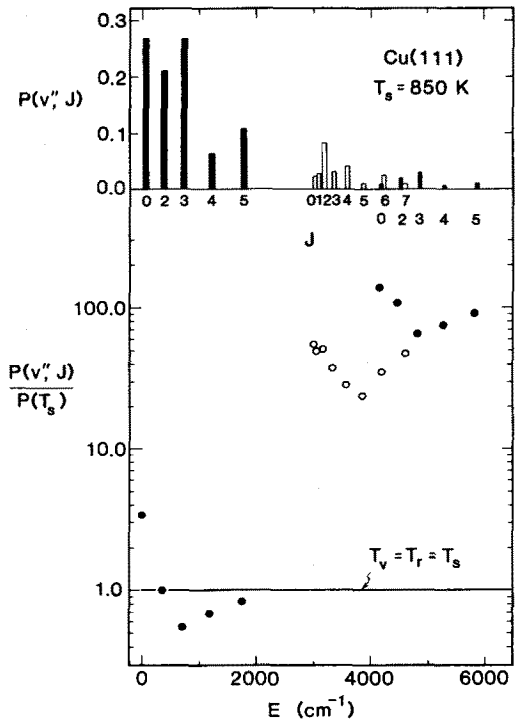

FIG. 9. Plot of the normalized rovibrational state distributions of H_2 and D_2 desorbing from Cu(111) at $T_s = 850$ K. The lower panel plots logarithmically the desorption distributions divided by the corresponding equilibrium-at-T_s distributions ($P(T_s)$). Solid bars and circles correspond to H_2; open ones to D_2.

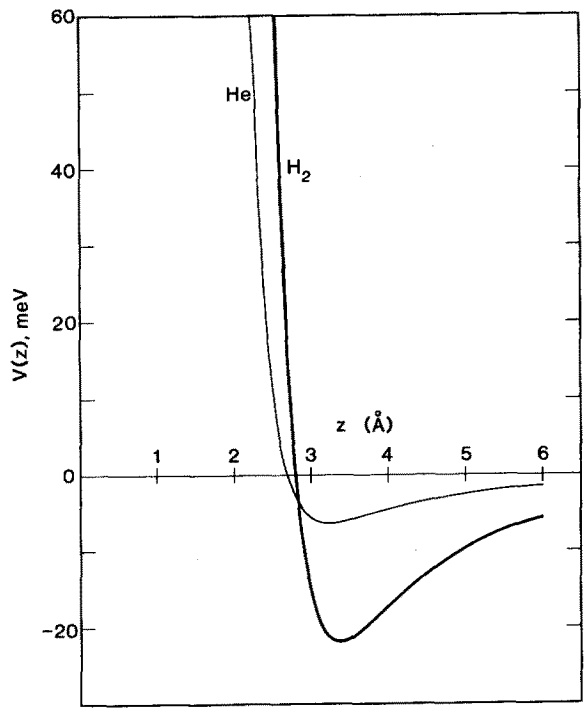

FIG. 10. Comparison of H_2/Cu and He/Cu laterally averaged 9-3 potential energy curves. Potential parameters taken from Perreau and Lapujoulade (Ref. 26).

In contrast to velocity and angular distributions in desorption, the results presented in Fig. 8 demonstrate that the molecular rotational degree of freedom is insensitive to the surface structural differences between the (110) and (111) planes. This may be understood using a simple approximate method to generate the H_2–Cu repulsive potentials.

The closed-shell character of molecular hydrogen gives rise to primarily repulsive interactions with metal surfaces. A pertinent example of this lies in selective adsorption and elastic scattering measurements of H_2 from Cu(110) and Cu(115).[26] These results yield an H_2/Cu(110) well depth, D, of only 22.0 ± 0.5 meV or ~ 0.5 kcal/mol. Therefore D is approximately 10 times less than the activation barrier to dissociative adsorption on copper. Also of interest is the fact that the repulsive limb of the laterally averaged H_2/Cu and He/Cu potentials appear to be quite similar when fit to the 9-3 form[26]:

$$V(z) = \tfrac{1}{2}\, 3^{3/2} D\, [(\sigma/z)^9 - (\sigma/z)^3], \tag{2}$$

where σ, the range parameter, is 2.7 Å for He and 2.8 Å for H_2. This is demonstrated in Fig. 10 where it is shown that the He and H_2 repulsive limbs appear to be nearly parallel (they are offset due the difference in van der Waals radii, $r_{H_2} - r_{He} \simeq 0.2$ Å). We make the chemically plausible assumption that the H_2/Cu repulsive potential can be qualitatively represented by that of He/Cu. We are motivated to make this approximation because of the extreme simplicity with which fairly accurate He/Cu repulsive energies can be determined.

Esjberg and Nørskov,[27] Laughlin,[28] and Batra *et al.*[29] have recently shown that, to a good approximation, repulsive interactions between a He atom and a target can be written

$$V = T \rho_{\text{target}}, \tag{3}$$

where $T \approx 1.0 \times 10^5$ meV Å^{-3} and ρ_{target} (charge Å^{-3}) is assumed to be uniform over the helium atom.

Equation (3) allows the repulsive He–metal potential to be trivially calculated once ρ_{target} is determined. We approximate[30] ρ_{target} using a superposition of Herman–Skillman atomic wave functions.[31] Although the Herman–Skillman wave functions are known to be less accurate in their tails than those wave functions calculated using the Kohn–Sham form of the exchange-correlation potential,[28] we believe that

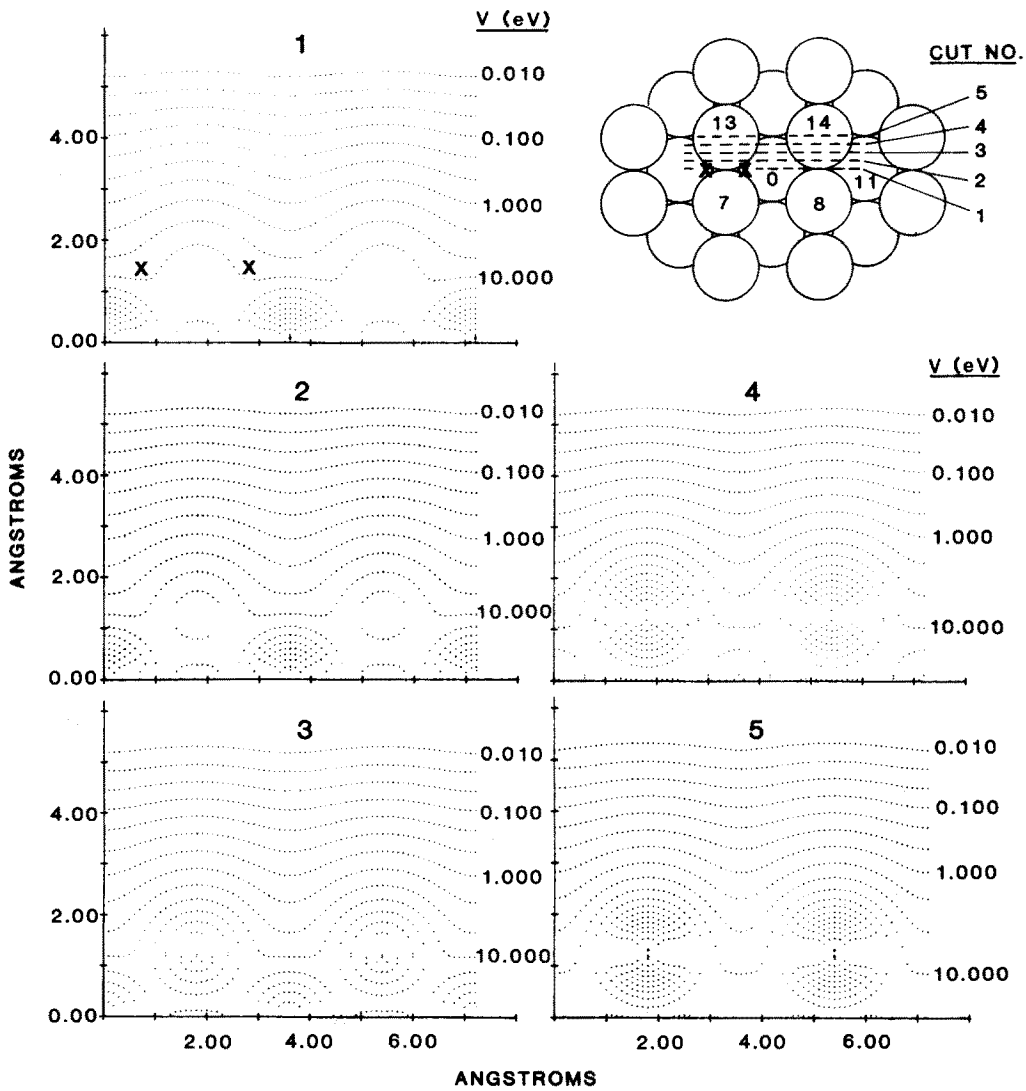

FIG. 11. Plots of Cu(110) electron isodensity contours calculated from the superposition of Herman–Skillman atomic Cu electron densities. The upper panel shows the 21 surface atoms used to generate the isodensity contours as well as the relationship between the cuts illustrated and these surface atoms. Distance normal to the surface is measured from the trough atom center. The ×'s approximately locate the H atom threefold binding sites.

this refinement is unwarranted given the level of the approximations already made.

The electron density at the surface is taken to be the sum of single atom electron densities appropriate to the known geometric structure of the surface. For the (110) face, 21 atoms are considered (see Fig. 11); 12 in the top atomic layer and 9 in the second. Figure 11 also shows the isodensity contour plots corresponding to the cuts sketched on the surface layer. The contour progression scales in increments of $10^{-1/3}$.

We compare in Fig. 12 the approximate H_2/Cu repulsive energies to those obtained by Madhavan and Whitten,[32] who used a 38 atom cluster and included configuration interaction. Figure 12 graphs the potential energy vs z, the distance above a fourfold site on the (100) face for the full CI calculations and the distance above sites A and B (see inset of Fig. 12) for our potential. We have assumed that the H–H internuclear separation remains fixed as z decreases, although it is likely that as the molecule approaches the surface the H_2 bond will stretch and the true molecule–surface repulsion will be reduced. The largest discrepancies between the Herman–Skillman superposition result and the full CI calculation occur at H_2–Cu distances less than ~ 1.4 Å where the repulsive energies of the former are approximately 0.6 eV higher above site A and 0.9 eV lower above site B than the latter. This is to be expected since the atomic superposition does not allow electron density to "spill out" over the surface away from the nuclear cores. The superposition calculation therefore yields metal electron densities which rise more sharply with decreasing z near a surface atom and more slowly with decreasing z between widely separated surface atoms (e.g., between atoms 7–8). Nonetheless, Fig. 12 demonstrates that the atomic superposition energies are likely to allow qualitatively meaningful conclusions to be reached regarding the repulsion experienced by a nascent hydrogen molecule after recombination.

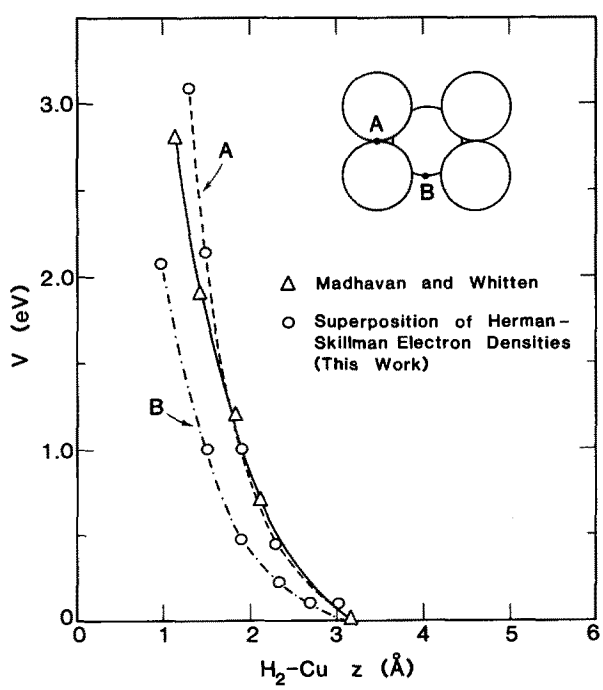

FIG. 12. Comparison of the simple H_2/Cu repulsive potentials shown in Fig. 10 with that calculated using configuration interaction by Madhavan and Whitten (Ref. 41) above a Cu(100) fourfold site. The inset shows the positions of the sites corresponding to curves A and B.

Computational results of Baskes and Daw[33] show that the threefold site in the (110) trough (shown as ×'s in Fig. 11) is the most stable H atom binding site on fcc metals such as Ni and Pt, and by inference Cu. The preferred H atom surface diffusion direction might therefore be along the troughs (in the [110] directions). The atom–atom encounter during recombination could then be imagined to occur with low impact parameter; the troughs impose a partial one-dimensional constraint on atomic diffusion. However this picture cannot explain our rotational results. Recall that the rotational distributions of H_2 and D_2 desorbing from *both* the (110) and (111) surfaces are "colder" than T_s and are identical for both faces. This experimental fact, combined with the (110) repulsive potentials diagrammed in Fig. 11 rules out this model. Assuming that the H–H internuclear separation is near its equilibrium value of 0.75 Å, in-trough recombination would form a molecule in a region corresponding to repulsive energies of 5–10 eV. At 1000 K, these energies are between 58–116 times greater than kT_s. Therefore, molecule formation at 1000 K must occur in regions with far less electron density than that found in the troughs.

Further inspection of Fig. 11 suggests that the insensitivity of the rotational distributions to crystal face can be understood from the repulsive-surface potentials as well. For example, molecule formation at a repulsive energy of 250 meV ($\sim 3kT_s$) occurs 3.75 Å above the (110) trough atoms ($r_{Cu-H} \sim 2.5$ Å). The maximum modulation of the potential in this region is only ~ 0.25 Å (in the [001] direction). On the close-packed (111) surface the modulation at this value of z will of course be closer to zero. The point is that the surface structural signature on the repulsive potential is obscured at these large values of z. The repulsive potentials, which can classically give rise to torques on the molecule, appear to be quite flat in the region where molecule formation probably occurs. If the torques applied to the nascent molecules are similar on both crystal faces, their rotational distributions will also be similar.

B. Vibrational and translational distributions and implications for detailed balance

In Sec. III C it was demonstrated that the $P_{v''=1}/P_{v''=0}$ population ratio is 58–93 times greater than that predicted for a Boltzmann vibrational distribution at $T = 850$ K. Similarly, the mean post-permeation desorption kinetic energy $\langle E_T \rangle$ is known to be ~ 4 times greater than for equilibrium desorption. We also know that the *adsorption probability* increases ~ 7 times as incident normal kinetic energy increases from 1 to 8 kcal/mol. Analogously, we ask if the post-permeation desorption vibrational population ratio implies, by detailed balance, that the adsorption probability for H_2 molecules excited to $v'' = 1$ is 58–93 times greater than for their $v'' = 0$ counterparts? This possibility is examined in what follows.

The concept of detailed balance can be stated in the following manner: for a system at equilibrium, the rate of for-

mation of a distinguishable macroscopic state and its reverse rate must be equal for a quantum system governed by transitions of random phase.[34] Notice that detailed balance applies only to systems *at equilibrium*. For nonequilibrium systems, microscopic reversibility allows one to state only that the forward and reverse transition probabilities connecting two quantum states are equal. At equilibrium, the summation over all the discrete transition probabilities is such that the forward and reverse rates for forming a distinct macroscopic state are balanced, i.e., the second law of thermodynamics is obeyed.

Although the concept of detailed balance rigorously applies only to equilibrium systems, it has been fruitfully applied to systems which clearly are not in equilibrium. An example can be found in the determination of the relative evaporation rates of tungsten and molybdenum oxides during molecular beam oxidation of the respective metal surfaces.[16] This "quasiequilibrium" method successfully predicted the various oxide desorption fluxes using only metal oxide thermochemical data, molecular oxygen incident flux, and T_s. An even more pertinent example is the previously mentioned detailed balance analysis of the molecular hydrogen/copper system.[5] In this example, *adsorption* probability data vs $E_\perp$ ($= \cos^2\theta_i \cdot E_i$) was used to predict *desorption* angular distributions. When detailed balance is unable to predict the properties of one process from properties associated with its apparent reverse process, the dynamics of these two processes must be different. We now reexamine the conclusion of Comsa and David[4] that post-permeation desorption and gas-phase adsorption experiments exhibit dissimilar dynamics. Additionally, we extend the detailed balance analysis to include molecular vibration.

Let us take the results of Balooch, Cardillo, Miller, and Stickney[8] (hereafter referred to as BCMS) for H_2 scattering from Cu(100) and attempt to calculate the angular dependence of the D_2 velocity distributions measured in recombinative desorption after atomic permeation by Comsa and David[4] (hereafter referred to as CD). We assume that the isotropic *variations* found in the adsorption probabilities ζ of D_2 and H_2 on Cu(110) by BCMS ($\zeta_{D_2} \sim 1.4\,\zeta_{H_2}$) can be applied to the Cu(100) face. To predict the CD results we take the flux-weighted dependence of ζ vs $E_\perp$, shown in Fig. 13, and multiply it by the flux-weighted Maxwellian distribution of velocities $P(v)$ at the surface temperature employed in the CD experiment. We calculate the equilibrium adsorption probability per unit area, $P(v,\theta_i)$, as a function of velocity at each value of the incident angle, θ_i, by determining the value of $E_\perp$ for a given (v,θ_i) combination, finding the corresponding value of ζ and multiplying it by $P(v)$. To compare directly with the CD results, the average kinetic energy, $\langle E_T \rangle$, of the adsorbing molecules is plotted vs θ_i in Fig. 14. If the equilibrium synthesis is valid for post-permeation desorption and gas-phase adsorption, detailed balance requires that the adsorption flux within any increment $dv\,d\theta_i$ is equal to the desorption flux into the same increment. The calculated values of $\langle E_T \rangle$ vs θ_s (see Fig. 14) would be identical to those measured by CD.

It is clear from Fig. 14 that the detailed balance construction fails to predict the values of $\langle E_T \rangle$ measured for

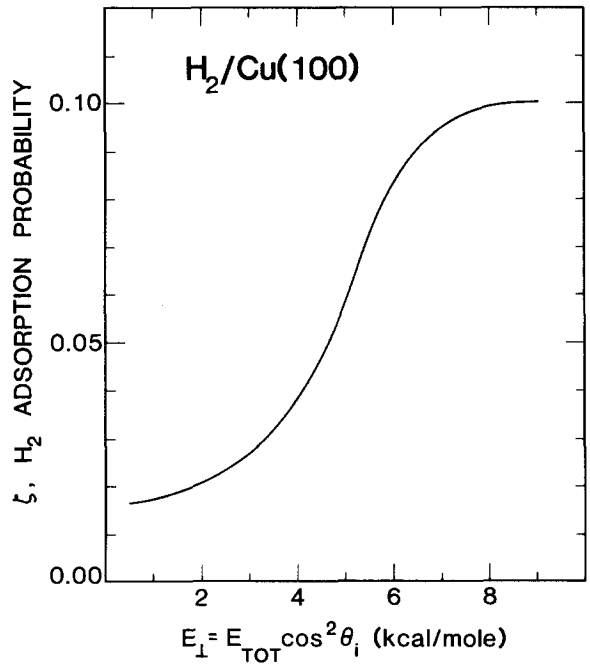

FIG. 13. Plot of the dissociative adsorption probability ζ vs the perpendicular component of incident kinetic energy for H_2 on Cu(100). Taken from Ref. 8.

post-permeation desorption. On average, the observed $\langle E_T \rangle$ values are ~ 2.5 times greater than the predicted ones. CD recognized this conflict and attempted to account for it with a model involving recombination of hydrogen *below* the surface. The possibility of subsurface recombination has been addressed in the last section.

As a further test of the applicability of detailed balance, we use the vibrational population results presented earlier and check for consistency with the data of BCMS. Are dyna-

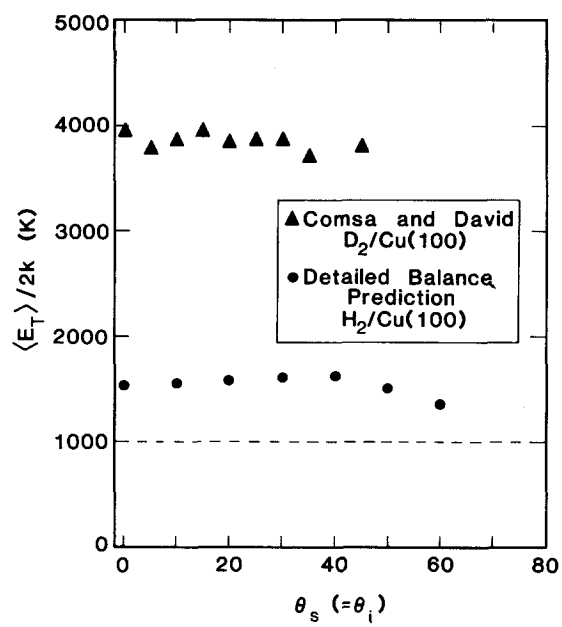

FIG. 14. Plot of the mean translational energy vs θ_s for D_2 recombinatively desorbing from Cu(100) measured by Comsa and David (Ref. 4). Also plotted is the detailed balance prediction of $\langle E_T \rangle$ vs θ_s calculated from the data of BCMS (Ref. 8).

mical differences also evident in the vibrational degree of freedom?

BCMS used a heated nozzle to obtain H_2 and D_2 beams of variable kinetic energy. At fixed $E_\perp$, higher nozzle temperatures must be employed for $\theta_i = 50°$, for example, than for $\theta_i = 25°$. In fact, since $\cos^2(50°) \approx 1/2 \cos^2(25°)$, $T_0(\theta_i = 50°) = 2T_0(\theta_i = 25°)$. The fractional population in $v'' = 1$ will therefore be systematically and appreciably greater for $\theta_i = 50°$ data than for $\theta_i = 25°$. Analyzing within a detailed balance framework the result that the ratio $P_{v''=1}/P_{v''=0}$ is ~ 50 times greater than for desorption in equilibrium at T_s, the adsorption probability for $v'' = 1$ molecules is predicted to be analogously enhanced relative to $v'' = 0$. This neglects possible correlations between vibration, desorption angle, and desorption velocity, which are still unknown. Writing the adsorption probability, $\zeta(E_\perp, v'')$, as proportional to $(P_{v''=0} + 50\,P_{v''=1}) \cdot f(E_\perp)$, using the relation $E_\perp = (5.37 \times 10^{-3}) T_0 \cdot \cos^2\theta_i$ quoted in BCMS, and assuming that $P_{v''=1} = \exp(-4161\ \text{cm}^{-1}/kT_0)$, we calculate the total adsorption probability for $\theta_i = 50°$. Figure 15 compares these values with the experimental data for $\theta_i = 50°$ and $\theta_i = 25°$. Also plotted is $f(E_\perp)$, the vibrationless contribution to $\zeta(E_\perp, v'')$. Here $f(E_\perp)$ is extracted from the $\theta_i = 25°$ data by dividing the experimental data by the function $(P_{v''=0} + 50\,P_{v''=1})$ at each value of T_0. In addition, we have assumed that the adsorption probability is independent of J because the measured rotational distributions show only mild departures from the thermal-at-T_s distributions. Inspection of Fig. 15 demonstrates that the detailed balance predictions and the data are once more in serious disagreement.

While correlations between molecular vibration and velocity and molecular vibration and θ_s may reduce the discrepancy between the permeation results and the adsorption probability data of BCMS, we believe[17] they cannot account for the differences illustrated in Fig. 14. We conclude that the translational and vibrational dynamics of these two processes are indeed dissimilar.

C. Features of the H_2/Cu potential manifested in molecular vibration

A possible cause for the observed dynamical differences between gas-phase adsorption and post-permeation desorption is suggested by the schematic potentials drawn in Fig. 16. The energy of atomic hydrogen dissolution in copper is 11.7 kcal/mol[35] and the activation energy for bulk diffusion is 9.3 kcal/mol.[36] A hydrogen atom diffusing to the surface from the selvedge region may therefore possess as much as 21 kcal/mol more energy than a free H_2 molecule in vacuum. It seems possible that a partially relaxed energetic atom reacts with a surface H atom to form a molecule before the energetic atom equilibrates in the H/Cu surface chemisorption well. Hydrogen atom relaxation at the surface might be relatively slow due to the large disparity between hydrogen atom and surface atom masses. In fact, this is borne out by recent molecular dynamics calculations[37] performed on accurate H/Ni potential surfaces, generated using the embedded atom method.[33] These calculations, which employ a 200 atom nickel slab and full lattice dynamics, demonstrate that an H atom with kinetic energy of 3000 K (260 meV) requires approximately 3 ps to relax to $\sim 2T_s$, for $T_s = 300$ K (ignoring relaxation from metal electronic excitation). This relaxation time corresponds to ~ 300 H–Ni "bounces". Therefore, some fraction of the diffusing atoms may recombine before full relaxation can occur, the excess energy appearing in the degrees-of-freedom of the newly formed molecule. Fully consistent with this idea are the observations that vibrational excitation *and* kinetic energy are much greater for post-permeation desorption than the detailed balance predictions

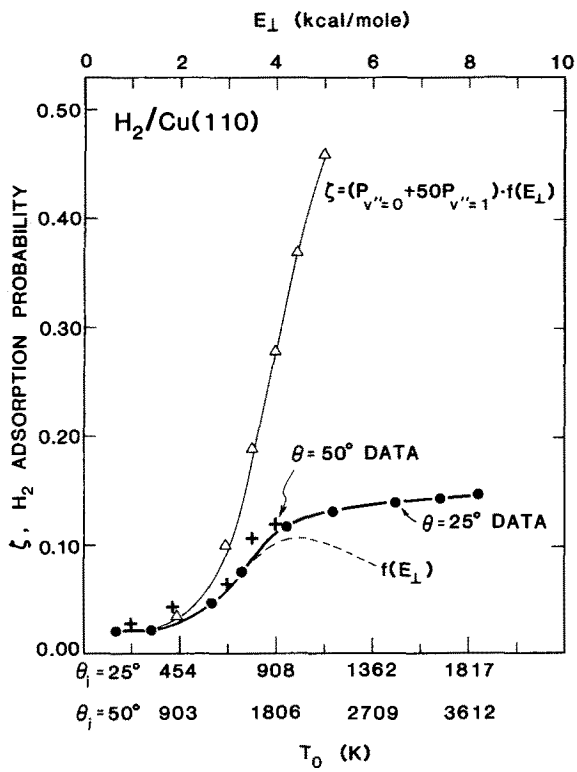

FIG. 15. Comparison of the H_2/Cu(110) adsorption probability data and the detailed balance prediction. The prediction uses the result that the $P_{v''=1}/P_{v''=0}$ ratio in desorption is ~ 50 times greater than the equilibrium-at-T_s value.

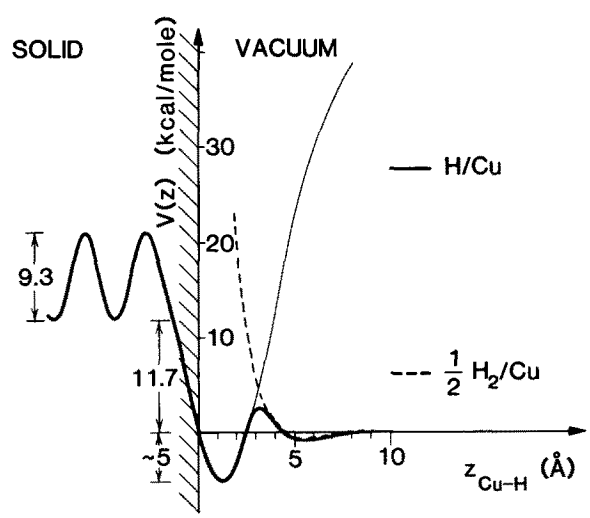

FIG. 16. Schematic one-dimensional potential energy curves for hydrogen on copper.

from adsorption data. The BCMS molecular beam results probe the activation barrier to chemisorption at a total energy which is less than half ($\sim$10 kcal/mol) of the presumed diffusing atom energy ($\sim$21 kcal/mol) in the permeation experiments.

It is interesting to note that the suggested maximum potential energy of the diffusing H atom, $\sim$21 kcal/mol, is slightly less than the energy for forming H_2 in $v''=2$, 23.2 kcal/mol. It is not surprising, therefore, that the population in H_2 $v''=2$ is so low as to escape detection. Only if two "hot" diffusing atoms were to react directly to form H_2 would there be sufficient energy to appreciably populate this level.

The precise mechanism of molecular hydrogen vibrational excitation resulting from the atomic encounters is at present unclear. A half-collision analog of the model recently proposed by Gadzuk,[38] however, may be pertinent.

Suppose the hydrogen atoms bound to the copper surface are partially negatively charged. As the partially charged atoms approach each other, they may be thought of as traveling on an H_2^-/Cu potential surface. If the combined kinetic energy of the two atoms is sufficient to surmount the activation barrier, they may do so upon molecule formation. This newly born molecule will travel upon the H_2^-/Cu potential for a short time as it increases its distance from the surface. At some point, an electron from H_2^- resonantly tunnels to one of the many unoccupied Cu levels above the Fermi energy. Depending on both the position of the image-stabilized H_2^- potential relative to that of H_2 at the time of electron jump and the total energy of the two atoms which formed the molecule, a vibrationally excited neutral molecule may be formed. The probability of $v''=1$ vs $v''=0$ formation may depend on the Franck–Condon factors between the H_2^- potential (which, because of its width does not have well-defined vibrational levels) and the vibrational levels of H_2. Of course, the Franck–Condon factors will be an appropriate description of these probabilities only if the change from ionic to neutral potentials is sudden.[39]

The calculations of Madhavan and Whitten[32] suggest that hydrogen atoms are partially negatively charged on copper. A Mulliken population analysis of H atoms chemisorbed to Cu(100) yields an H charge of $\sim$0.7. Because of limitations in the applicability of Mulliken populations, the authors argue that a charge of $\sim$0.3 per atom may be more likely. Even when the two atoms are bound to each other these authors state: "On stretching H_2, however, considerable [electronic] charge transfer to hydrogen occurs, primarily from the surface layer... ."[32] The hypothesis that the newly formed molecule travels temporarily on the negative ion potential surface is supported by these computational results.

It is expected that such an ion–neutral curve-crossing mechanism would depend sensitively on the surface work function. We have previously reported[7] the effects of a sulfur overlayer on the $P_{v''=1}/P_{v''=0}$ ratio where it was shown that this ratio *decreases sharply* for desorption from fresh sulfur-covered Cu(111). The work function of the slightly different Cu(100) surface increases from 4.77 eV when clean to 5.05 eV when covered with a $p(2\times2)$ sulfur adlayer.[40] In contrast to the clean copper surface, hydrogen atoms would not be expected to carry significant excess electron density on this more electronegative sulfur-covered surface. The proposed decay of the temporary negative ion into excited neutral molecular vibrational states would not be expected to occur in this case and a sharp diminution of $v''=1$ population could result. Although the recombinative desorption dynamics from sulfur-covered copper may be affected in a considerably more complex fashion than that just described, the work function trend is suggestive.

If temporary negative ion formation is an important component to the H_2/Cu desorption dynamics, then one may predict appreciable vibrational excitation of scattered H_2 molecules at incident energies greater than $E_{v''=1}$. The excitation mechanism is analogous to that just described and has recently been proposed by Gadzuk.[38,39] The lowering of the molecular affinity level allows resonant electron tunneling from the approaching metal to occur, temporarily forming H_2^-. After rebounding from the surface, the electron tunnels back to the metal, leaving H_2 in one or more vibrationally excited levels (subject to the incident beam energy). Hence, H_2 (or D_2) beam scattering experiments at incident energies greater than 0.52 eV (0.37 eV) might prove to be a sensitive test of the importance of negative molecular ion formation in the hydrogen/copper system. A method to produce translationally "hot" but vibrationally "cold" molecular hydrogen beams would be required to detect the expected $v''=0\rightarrow v''=1$ excitation, however.

We have shown that the dynamics of post-permeation desorption and gas-phase adsorption cannot be accurately compared using detailed balance. The qualitative dynamical trends, however, seems to be preserved. Therefore, it is interesting to compare the current experiment with the dynamical trends predicted by Gelb and Cardillo,[40] in a series of LEPS calculations of the dissociative adsorption probability as functions of vibration, rotation, and velocity. They concluded that the adsorption probability is insensitive to rotational excitation but increases sharply with vibrational excitation. In desorption, therefore, the predicted rotational distributions would be close to Boltzmann at T_s but the vibrational distributions would be considerably more energetic than their Boltzmann-at-T_s counterparts. These are the dynamical trends observed in the present study.

V. CONCLUSIONS

The rotational and vibrational distributions of H_2 and D_2 recombinatively desorbing from Cu(110) and Cu(111) after permeation have been determined using resonance-enhanced 2 + 1 multiphoton ionization. Rotational distributions are found to be non-Boltzmann with mean rotational energies slightly less than T_s. These distributions are invariant with respect to crystallographic surface orientation and molecular isotope. In contrast, the $P_{v''=1}/P_{v''=0}$ population ratios are found to be 50–90 times greater than the Boltzmann-at-T_s values. This ratio is larger for desorption from Cu(111) than from Cu(110). Thus, the vibrational degree of freedom plays a major role in the desorption dynamics, whereas rotation does not. It is interesting to note that classical trajectory calculations performed by Gelb and Cardillo[41]

reached qualitatively similar conclusions for the relative importance of rotation and vibration in adsorption.

Approximate H_2/Cu repulsive potentials have been calculated. They are used to suggest that recombination occurs in regions sufficiently far above the plane of surface atoms such that surface structural modulation of the potential is weak. It is inferred from a detailed balance analysis that the dynamics of post-permeation desorption and gas-phase adsorption differ, and that these differences are manifested in vibrational as well as translational degrees of freedom. Finally, the surface-mediated formation of a temporary negative ion (H_2^-) offers an appealing interpretation for the mechanism of vibrational excitation.

ACKNOWLEDGMENTS

We are grateful to Dr. M. J. Cardillo, Dr. S. M. Foiles, Dr. C. T. Rettner, and Dr. A. E. DePristo for helpful discussions during the course of this work. We also thank Mr. M. Gutierrez for the expertise he contributed to the permeation source construction. G. D. Kubiak acknowledges partial support from the Grace Foundation. This work is supported in part by the Army Research Office under Grant No. DAAG-29-84-K-0027, and in part by the Office of Naval Research under Grant No. N00014-78-C-0403.

[1]See J. R. Barker and D. J. Auerbach, Prog. Surf. Sci. (to be published).
[2]T. L. Bradley and R. E. Stickney, Surf. Sci. **38**, 313 (1973).
[3]M. Balooch and R. E. Stickney, Surf. Sci. **44**, 310 (1974).
[4](a) G. Cosma and R. David, Surf. Sci. **117**, 77 (1982); (b) G. Cosma, in *Dynamics of Gas–Surface Interaction*, edited by G. Benedek and U. Valbusa (Springer, Berlin, 1982).
[5]M. J. Cardillo, M. Balooch, and R. E. Stickney, Surf. Sci. **50**, 263 (1975).
[6]G. D. Kubiak, G. O. Sitz, and R. N. Zare, J. Chem. Phys. **81**, 6397 (1984).
[7]G. D. Kubiak, G. O. Sitz, and R. N. Zare, J. Vac. Sci. Technol. A **3**, 1649 (1985).
[8]M. Balooch, M. J. Cardillo, D. R. Miller, and R. E. Stickney, Surf. Sci. **46**, 358 (1974).
[9]J. Pritchard and F. C. Tompkins, Trans. Faraday Soc. **56**, 540 (1960).
[10]J. Pritchard, Trans. Faraday Soc. **59**, 437 (1963).
[11]C. S. Alexander and J. Pritchard, J. Chem. Soc. Faraday Trans. **68**, 202 (1972).
[12]J. Pritchard, T. Catterick, and R. K. Gupta, Surf. Sci. **53**, 1 (1975).
[13]I. E. Wachs and R. J. Madix, Surf. Sci. **84**, 375 (1979).
[14]J. E. Lennard-Jones, Trans. Faraday Soc. **28**, 333 (1932).
[15]W. van Willigen, Phys. Lett. A **28**, 80 (1968).
[16]J. C. Batty and R. E. Stickney, MIT Technical Report #473, 1969.
[17]G. D. Kubiak, Ph.D. thesis, Stanford University, Stanford, CA, 1984.
[18](a) E. E. Marinero, C. T. Rettner, and R. N. Zare, Phys. Rev. Lett. **48**, 1323 (1982); (b) E. E. Marinero, R. Vasudev, and R. N. Zare, J. Chem. Phys. **78**, 692 (1983); (c) S. L. Anderson, G. D. Kubiak, and R. N. Zare, Chem. Phys. Lett. **105**, 22 (1984).
[19]G. Golovchenko (private communication).
[20]J. S. Ahearn, Jr., and J. P. Mitchell, Rev. Sci. Instrum. **41**, 1853 (1970).
[21]For reasons which are not clear, positioning the input lens in such a way as to cause the laser to pass ~6 mm off the optical axis approximately doubles the AS_4 energy. The expected "stretching out" of the laser focus caused by spherical aberration in the lens may play a role in this effect.
[22]R. J. Gallagher and J. B. Fenn, J. Chem. Phys. **60**, 3492 (1974).
[23]G. D. Kubiak, J. E. Hurst, Jr., H. G. Rennagel, G. M. McClelland, and R. N. Zare, J. Chem. Phys. **79**, 5163 (1983).
[24]R. B. Gerber, L. H. Beard, and D. J. Kouri, J. Chem. Phys. **74**, 4709 (1981).
[25]R. G. Bray and R. M. Hochstrasser, Mol. Phys. **31**, 1199 (1975).
[26]J. Perreau and J. Lapujoulade, Surf. Sci. **122**, 341 (1982).
[27]N. Esjberg and J. Nørskov, Phys. Rev. Lett. **45**, 807 (1980); see also E. Zaremba and W. Kohn, Phys. Rev. B **15**, 1769 (1977).
[28]R. B. Laughlin, Phys. Rev. B **25**, 2222 (1982).
[29]I. P. Batra, P. S. Bagus, and J. A. Barker, Phys. Rev. B **31**, 1737 (1985).
[30]D. Haneman and R. Haydock, J. Vac. Sci. Technol. **21**, 330 (1982); but see also N. Garcia, J. A. Barker, and I. P. Batra, J. Electron. Spectrosc. **30**, 137 (1983); Solid State Commun. **47**, 485 (1983).
[31]F. Herman and S. Skillman, *Atomic Structure Tables* (Prentice–Hall, Englewood Cliffs, 1963).
[32]P. Madhavan and J. L. Whitten, J. Chem. Phys. **77**, 2673 (1982).
[33]M. S. Daw and M. I. Baskes, Phys. Rev. B **29**, 6443 (1984).
[34]R. Tolman, *The Principles of Statistical Mechanics* (Oxford University, Oxford, 1967).
[35]E. Fromm and E. Gebhardt, *Gase und Kohlenstoff in Metallen* (Springer, Berlin, 1976), p. 658.
[36]L. Katz, M. Guinan, and R. J. Borg, Phys. Rev. B **4**, 330 (1971).
[37]Stephen M. Foiles (unpublished results).
[38](a) J. W. Gadzuk, J. Chem. Phys. **79**, 6341 (1983); (b) J. W. Gadzuk and J. K. Nørskov, *ibid.* **81**, 2828 (1984).
[39](a) J. W. Gadzuk, J. Chem. Phys. **79**, 3982 (1983); (b) Phys. Rev. B **20**, 515 (1979).
[40]G. G. Tibbetts, J. M. Burkstrand, and J. C. Tracy, Phys. Rev. B **15**, 3652 (1977).
[41](a) A. Gelb and M. J. Cardillo, Surf. Sci. **59**, 128 (1975); (b) **64**, 197 (1977); (c) **75**, 199 (1978).